Earthquakes and Structures, *Vol. 6, No. 1 (2014) 019-043*
DOI: http://dx.doi.org/10.12989/eas.2014.6.1.019

Risk assessment of steel and steel-concrete composite 3D buildings considering sources of uncertainty

Nikos D. Lagaros*

Institute of Structural Analysis & Antiseismic Research, Department of Structural Engineering, School of Civil Engineering, National Technical University Athens, 9, Iroon Polytechniou Str., Zografou Campus, GR-15780 Athens, Greece

(Received March 20, 2013, Revised August 20, 2013, Accepted September 22, 2013)

Abstract. A risk assessment framework for evaluating building structures is implemented in this study. This framework allows considering sources of uncertainty both on structural capacity and seismic demand. In particular randomness on seismic load, incident angle, material properties, floor mass and structural damping are considered; in addition the choice of fibre modelling versus plastic hinge model is also considered as a source of uncertainty. The main objective of this work is to study the contribution of these sources of uncertainty on the fragilities of steel and steel-reinforced concrete composite 3D building structures. The fragility curves are expressed in the form of a two-parameter lognormal distribution where vertical statistics in conjunction with metaheuristic optimization are implemented for calculating the two parameters.

Keywords: aleatory and epistemic uncertainties; fragilities; fibre and plastic hinge modelling; multicomponent incremental dynamic analysis; steel and steel-concrete composite buildings

1. Introduction

During the last decades, risk management has gained the attention of economic and technical decision centres in modern society. Proper tools for estimating the consequences of natural hazardous events on built environment and thus to propose optimal allocation of public resources for sustainable economy are required. Risk management addresses this claim indicating the procedure to implement optimal choices. Risk assessment and decision analysis are the main steps of risk management concept. The main ingredient of risk assessment procedure is seismic fragility analysis, resulting to limit-state probabilities of exceedance as functions of earthquake ground motion intensity.

A number of studies on structural fragility analysis have been published so far. Kennedy *et al*. (1980) determined the probability of earthquake induced radioactive releases resulted from core melt. Kircher *et al*. (1997) based on earthquake loss estimation methodology by Federal Emergency Management Agency-National Institute of Building Sciences (FEMA/NIBS) presented the description of building damage functions. Shinozuka *et al*. (2003) developed fragility curves

*Professor, E-mail: nlagaros@central.ntua.gr

 ISSN: 2092-7614 (Print), 2092-7622 (Online)

for bridges, aiming to determine the earthquakes effect on transportation network systems' performance. Gardoni *et al*. (2003) developed a methodology for defining probabilistic seismic demand models for structural systems' components in order to estimate seismic fragilities of bridge components. Wen and Ellingwood (2005) studied the importance of fragility analysis in various stages of consequence based engineering. Pagni and Lowes (2006) developed fragility functions aiming to assess methods for repairing old reinforced concrete (RC) beam to column joints damaged due to earthquake loading. Kappos *et al.* (2006) presented a methodology for assessing unreinforced masonry and reinforced concrete (RC) structures based on fragility analysis. Based on fundamental response quantities of stiffness, strength and ductility, Jeong and Elnashai (2007) derived a set of fragility relationships with known reliability; for this purpose the fundamental response quantities of a wide range of structural systems was defined and the fragility relationships for various limit states were constructed. Porter *et al.* (2007) introduced procedures for creating fragility functions from various kinds of data like the actual engineering demand parameter (EDP) at which each specimen failed, bounding EDP, capable EDP, expert opinion and others. Lagaros (2008) used fragility analysis in order to assess the structural performance of RC structures obtained implementing three design practices and varying the behaviour factor value used to define the seismic design forces. Eleftheriadou and Karabinis (2012) presented a study on the seismic vulnerability assessment of typical building types, representative of the structural materials, the seismic codes and the construction techniques of Southern Europe, in this direction a damage database was created after the elaboration of the results of data observed from post-earthquake surveys carried out in the area struck by the September 7, 1999 Athens earthquake.

Real-world structures are characterized by imperfections while material properties and loading conditions are uncertain, which induce deviations from their nominal state assumed by the design codes. A deterministic representation of a design that ignores scatter of any kind of the parameters affecting its response is never materialized in an absolute way, due to unavoidable scattering of the values of its parameters. So far a number of researchers studied the effect of uncertainties in the context of fragility analysis; mainly in steel and RC structures. A statistical analysis procedure of fragility curves of RC bridges was presented by Shinozuka *et al.* (2000), while Ellingwood (2001) examined the significance of inherent randomness and modelling uncertainty in forecasting the building performance by means of fragility assessment. A procedure to account for the uncertainty in the characteristics of future ground motions during seismic response assessment was presented in the work by Aslani and Miranda (2005) for RC structures. Assessments of collapse risk of RC moment frame buildings considering uncertainties in structural component strength, stiffness, deformation capacity and cyclic deterioration was carried out by Liel *et al*. (2009). Celik and Ellingwood (2010) presented a study of the contribution of uncertainties in material and structural parameters that revealed that structural damping, concrete strength, and cracking strain in beam to column joints have the greatest impact on the fragilities of RC frames. Aygün *et al*. (2011) presented a computationally efficient approach in order to study the uncertainty propagation on the fragility of coupled bridge-soil-foundation system components. Kim *et al*. (2011) studied a methodology considering inherent randomness and modelling uncertainty of component fragilities of nuclear power plants.

The main objective of the present study is to study the influence of various sources of uncertainty on the fragilities of steel and steel-reinforced concrete composite 3D buildings in a more systematic approach. Four 3D buildings are considered while randomness on seismic demand and incident angle along with uncertainty on material properties, floor mass and structural

damping is taken into account. An important source of uncertainty is the modelling approach adopted, for this purpose the choice of fibre modelling versus the plastic hinge model is also considered as a source of uncertainty. The fragility curves are expressed in the form of a two-parameter lognormal distribution where a metaheuristic optimization algorithm is implemented for calculating the two parameters, in the context of vertical statistics and the maximum likelihood method, as suggested by Mitropoulou and Papadrakakis (2011). In this work the Differential Evolution (DE) algorithm, proposed by Storn and Price (1997), is adopted. The contribution of the sources of uncertainty is examined by means of multicomponent incremental dynamic analysis (MIDA) (Lagaros 2010), where 100 seismic events recorded in the area of the city of San Diego, California (Latitude (N) 32.7^o, Longitude (W) -117.2^o) are considered.

2. Fragility analysis

Earthquake risk assessment of structures requires the calculation of limit-state probabilities for a series of limit-states. Fragility analysis provides a measure of the safety margin of structural systems and is considered the main ingredient of earthquake risk assessment. The mean annual frequency of maximum EDP value (like interstorey drift $\theta_{\max}$) exceeding a value y is obtained as

$$v_{EDP>y} = \int P\left(EDP_{\max} \geq y / IM = x\right) \left| d\lambda_{IM}\left(x\right) \right| \tag{1}$$

where $v_{\mathrm{EDP>y}}$ is the rate of $EDP_{\max}$, exceeding the value y and $\lambda_{IM}(x)$ is the hazard curve representing the mean annual frequency of the chosen intensity measure exceeding x. The absolute value is used for the slope because it has a negative value.

According to Eq. (1) the seismic fragility F_R is defined as the limit-state probability, conditioned on a measure of seismic intensity *IM*, like the peak ground acceleration, spectral acceleration, spectral velocity, or any other measure that is consistent with the specification of seismic hazard. The IM should be a monotonically scalable ground motion intensity measure like the peak ground acceleration (PGA), peak ground velocity (PGV), the ξ=5% damped spectral acceleration at the structure's first-mode period ($S_A(T_1,5\%)$), among others. In the current work the $S_A(T_1,5\%)$ is selected, since it is the most commonly used intensity measure in practice today for the analysis of buildings. The seismic fragility curves are defined as

$$F_R = P\left(EDP_{\max} \geq y / IM = x\right) \tag{2}$$

According to Shinozuka *et al.* (2000) it is assumed that the curves F_R can be expressed in the form of two-parameter (median-μ and log-standard deviation-β) lognormal distribution functions, and the estimation of the two parameters is performed by means of the maximum likelihood method. The likelihood function for the present purpose is expressed as follows (2002)

$$L(\mu_1, \mu_2, \ldots, \mu_n, \beta_1, \beta_2, \ldots, \beta_n) = \prod_{i=1}^{N} \prod_{k=1}^{n} F_R(S_{A,i}, y_k)^{x_{ik}} \tag{3}$$

where F_R represents the fragility curve for a specific state of damage; $S_{A,i}$ is the first mode spectral acceleration value to which the ith realization of the structure is subjected; x_{ik} is equal to 1 or 0 depending on whether or not the ith realization of the structure sustains the state of damage under

$S_{A,i}$; N is the total number of structural realizations after the earthquake and n is the total number of the limit-states considered. Therefore, F_R, for the kth limit-state, takes the following form

$$F_{R,k}(S_A) = \Phi\left[\frac{ln(S_A / \mu_k)}{\beta_k}\right] \tag{4}$$

in which Φ is the standardized normal distribution function. As suggested by Shinozuka *et al.* (2000) the two parameters μ and β of Eq. (4) are computed as the values that maximize ln(L) by implementing a straightforward optimization algorithm. The advantage of the likelihood function of Eq. (3) that was employed in this study is that the parameters of the fragilities for all limit-states considered are obtained through a single optimization run. In this work a metaheuristic optimization algorithm (Mitropoulou *et al.* 2010, Fragiadakis and Lagaros 2011) is applied where no gradient evaluations are required. In particular the DE algorithm is employed since it was found to be robust and efficient in a number of engineering problems (Lagaros and Karlaftis 2011, Lagaros and Papadrakakis 2012). For this purpose MIDA that is used for developing the dynamic capacity curves taking into account the influence of earthquake incident angle and that of sources of uncertainty along with "Vertical" statistics are used to quantify the ground motion intensity at which a system approaches a certain limit-state.

3. Description of the structural models

In this work, two 3D steel and two 3D steel-RC composite buildings (Fig. 1) have been considered in order to study the influence of various sources of uncertainty on the fragility analysis of structures. For both steel and steel-RC composite test examples correspond to buildings with four and eight storeys having symmetrical plan view. All four buildings have been designed according to the specification for structural steel and composite buildings ANSI/AISC 341-10 (2010), since the four buildings are considered to be constructed in the city of San Diego (Latitude (N) 32.7^o, Longitude (W) -117.2^o), while all beam to column joints were considered as rigid. Concrete of class with nominal cylindrical compressive strength of 20 MPa (corresponding to the moderately confined concrete of the composite section, see Fig. 2) with modulus of elasticity equal to 30 GPa, steel reinforcement of class with nominal yield stress of 500 MPa and structural steel of class with nominal yield stress of 235 MPa; both with modulus of elasticity equal to 200 GPa are considered. Compared to the moderately confined concrete the cylindrical strength of the unconfined concrete is reduced by 20% while that of the highly confined one is increased by 10%. The cross section of the beams for all buildings is IPE240, while the bracings are L100×10. The cross sections of the columns for the steel buildings are HEB360 (4 storeys building) and HEB450 (8 storeys building), while for the composite ones HEB300 encased in concrete rectangular section 50×50 cm^2 (4 storeys building) and HEB340 encased in concrete rectangular section 55×55 cm^2 (8 storeys building). The slab thickness is equal to 12 cm, while in addition to the self-weight of beams and slabs, a distributed permanent load of 2 kN/m^2 due to floor finishing partitions and an imposed load of 1.5 kN/m^2, are considered. The small thickness of the slabs is justified by the fact that secondary beams that support the slab are used, while they are not introduced in the numerical models. The connection between beam and slab was considered using a number of stud connectors welded to the top flange of the steel beams, the composite action though was ignored because the spacing of the shear connectors was not considered sufficient (ANSI/AISC 341-10 2010). The

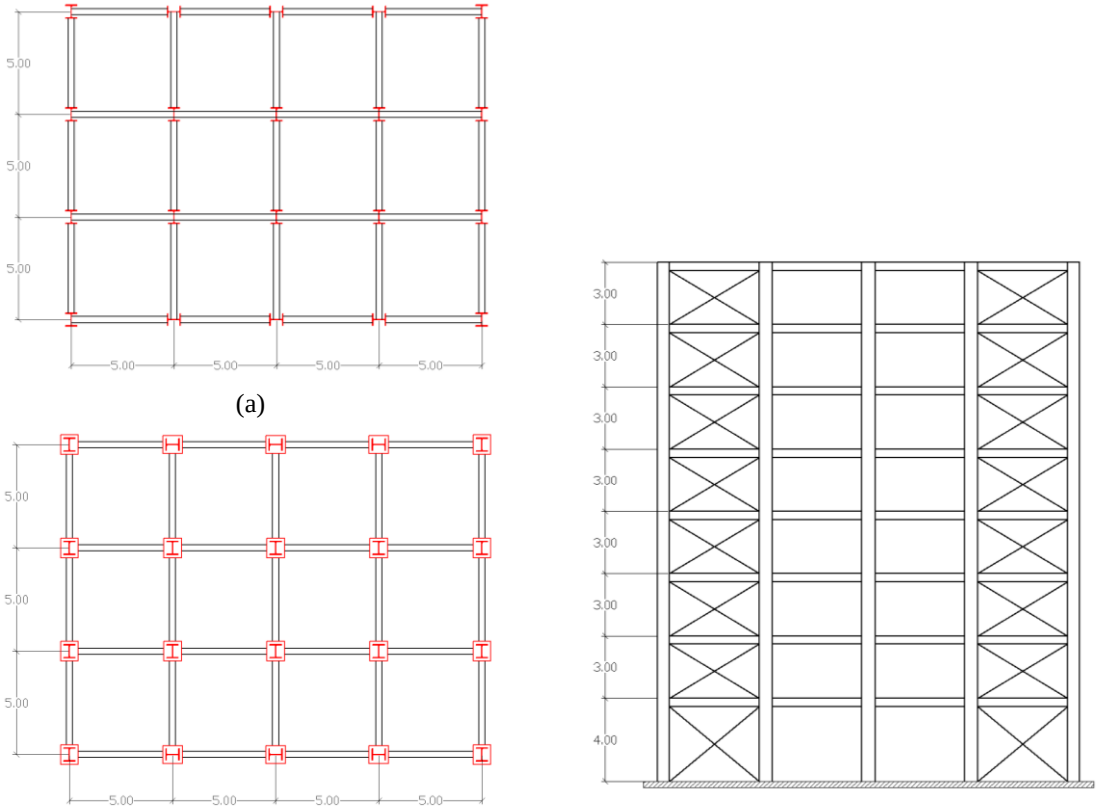

(a) (b) (c)

Fig. 1 Test examples - (a) steel building plan view, (b) steel-reinforced concrete composite building plan view and (c) eight storey steel building front view

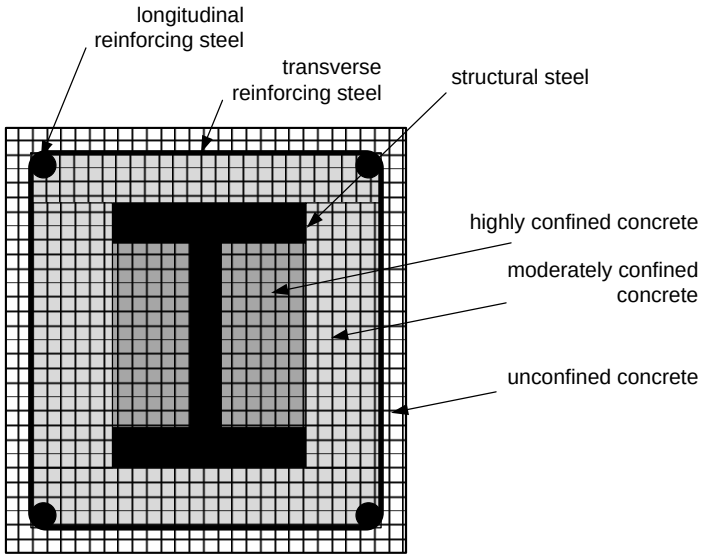

Fig. 2 Fibre discretization of a steel-reinforced concrete composite section

fundamental vibration periods for the nominal values of the material properties are 1.7 seconds for the 4 storey steel building, 2.4 seconds for the 8 storey steel one, 1.0 seconds for the 4 storey steel-RC composite and 2.3 seconds for the 8 storey steel-RC composite building.

4. Modelling and finite element analysis

Nonlinear static or dynamic analysis needs a detailed simulation of the structure in the regions where inelastic deformations are expected to develop. The inelastic behaviour is considered either by means of plastic hinge or fibre approach. For some researchers plastic hinge approach has limitations in terms of accuracy and therefore fibre beam-column elements are preferred (Fragiadakis and Papadrakakis 2008).

According to the fibre approach, each structural element is discretized into a number of integration sections restrained to the beam kinematics, and each section is divided into a number of fibres (Fig. 3) with specific material properties (A_{fib}, E_{fib}). Every fibre in the section can be assigned to different material properties, e.g. concrete, structural steel, or reinforcing bar material properties (see Fig. 2 for the case of a composite column). The sections are located at the Gaussian integration points of the elements. According to the fibre approach, every fibre has a simple uniaxial material model allowing an easy implementation of the inelastic behaviour. This approach is considered to be suitable for inelastic beam-column elements under dynamic loading and provides a reliable solution compared to other formulations (Fragiadakis and Papadrakakis 2008). The plastic hinge formulation is implemented with the "beamWithHinges" element of OpenSees (McKenna and Fenves 2001), which is based on the flexibility formulation, and considers plasticity to be concentrated over specified hinge lengths at the element ends as it is described in Scott and Fenves (2006). The plastic hinge integration implemented in this study is based on the assumption that the nonlinear constitutive behaviour is confined to the regions of length L_p at the elements ends, while the Gauss-Radau plastic hinge integration, proposed by Scott and Fenves (2006), is implemented. According to Hauke *et al.* (2008) the plastic hinge length for both steel and steel-RC buildings is suggested to be equal to two times the height of the cross section, since a sufficient correlation with test results were obtained for estimating the plastic hinge length in their parametric study.

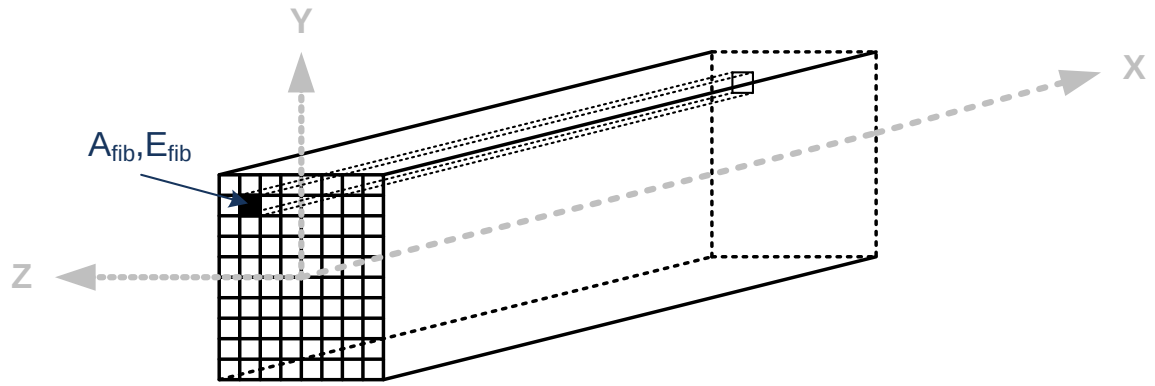

Fig. 3 Modelling of the inelastic behaviour-the fibre approach

In the numerical test examples section that follows all analyses have been performed using the OpenSees (McKenna and Fenves 2001) platform. A bilinear material model with pure kinematic hardening is adopted for the structural steel (Steel01 (McKenna and Fenves 2001)), while geometric nonlinearity is explicitly taken into consideration. For the simulation of the concrete the modified Kent-Park model, where the monotonic envelope of concrete in compression follows the model of Kent and Park (1971) as extended by Scott *et al*. in (1982), is employed (Concrete02 (McKenna and Fenves 2001)). This model was chosen because it allows for an accurate prediction of the demand for flexure-dominated RC members despite its relatively simple formulation. The bracing members are modelled using an inelastic element with pinned ends (Tremblay 2002), while the transient behaviour of the reinforcing bars was simulated with the Menegotto-Pinto model (Menegotto and Pinto 1973, Steel02 (McKenna and Fenves 2001).

The static pushover capacity curves for the nominal values of the material properties and zero steel hardening are shown in Figs. 4 and 5. In these Figures the efficiency of the plastic hinge Gauss-Radau modelling with reference to the force-based element with Gauss-Lobatto integration is examined. For this purpose three different lengths of the plastic hinge are considered (one, two and four times the height of the cross section) while 2, 4 and 8 integrations points for both beams and columns are considered for the Gauss-Lobatto integration. The computed response for the two modelling types is quite close for all buildings especially when the plastic hinge length is equal to four times the height of the cross section. In order to compromise accuracy with computationally efficiency, for the dynamic analyses that are carried out in this study 4 integration points are considered while the plastic hinge length is considered to be equal to four times the height of the cross section.

5. Uncertain parameters

It is common in earthquake risk analysis to distinguish between uncertainty that reflects the variability of the outcome of a repeatable experiment and uncertainty due to ignorance. The last one is sometimes referred as "randomness", commonly known as "aleatory uncertainty", which cannot be reduced. However, both deterministic and probabilistic approaches rely on various model assumptions and model parameters that are based on the current state of knowledge on the behaviour of structural systems under given conditions. There is uncertainty associated with these conditions, which depends upon the state of knowledge that is referred as "epistemic uncertainty".

In this study various sources of uncertainty are considered: on the ground motion excitation (aleatoric randomness) which influences the level of seismic demand and on the modelling (epistemic uncertainty) which affects the structural capacity. The structural stiffness is directly connected to the modulus of elasticity E_s, $E_{s,r}$ and E_c of the structural steel, reinforcement steel and concrete respectively, while the strength is influenced by the yield stress f_y, $f_{y,r}$ of the structural steel, reinforcement steel and the cylindrical strength for the concrete f_c and the hardening (b and b_r) of the steel. In addition to the above mentioned material properties, the mass and the damping are considered as random variables. Thus, for the columns three random variables are considered for the steel buildings and eight for the composite buildings; the modulus of elasticity (E_s, $E_{s,r}$ and E_c), the yield and cylindrical strength stresses (f_y, $f_{y,r}$ and f_c) and the hardening parameter b (structural steel) and b_r (reinforcement steel) of the stress-strain curve, while for the beams the modulus of elasticity E_s, the yield stress f_y and the hardening parameter b are considered as random variables. The material properties parameters for the steel reinforcement and the structural steel of

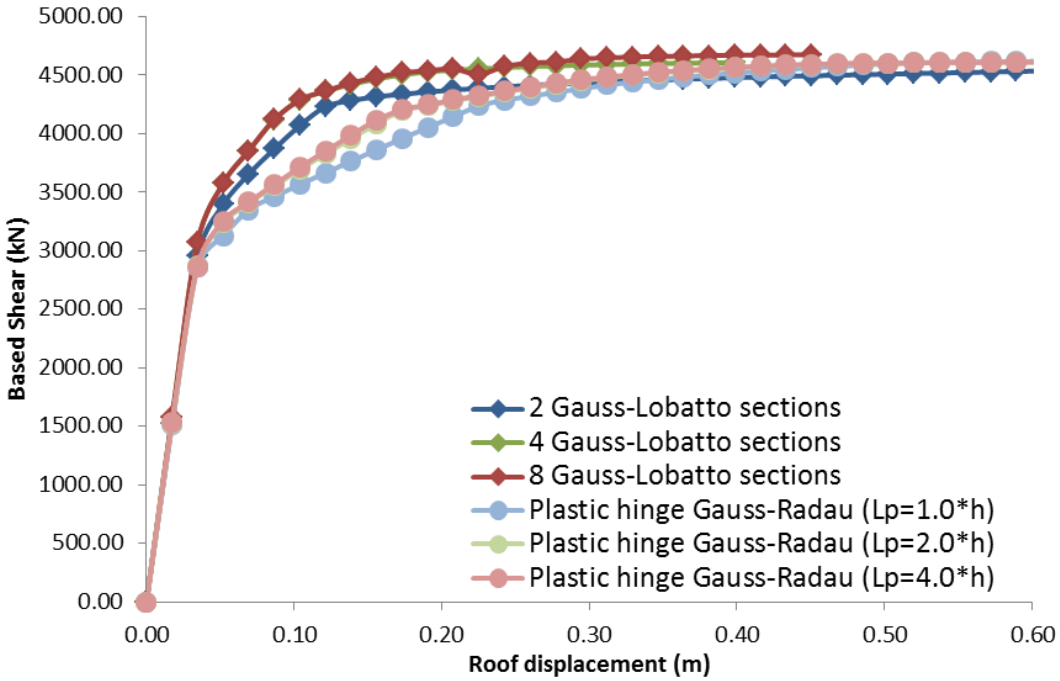

(a)

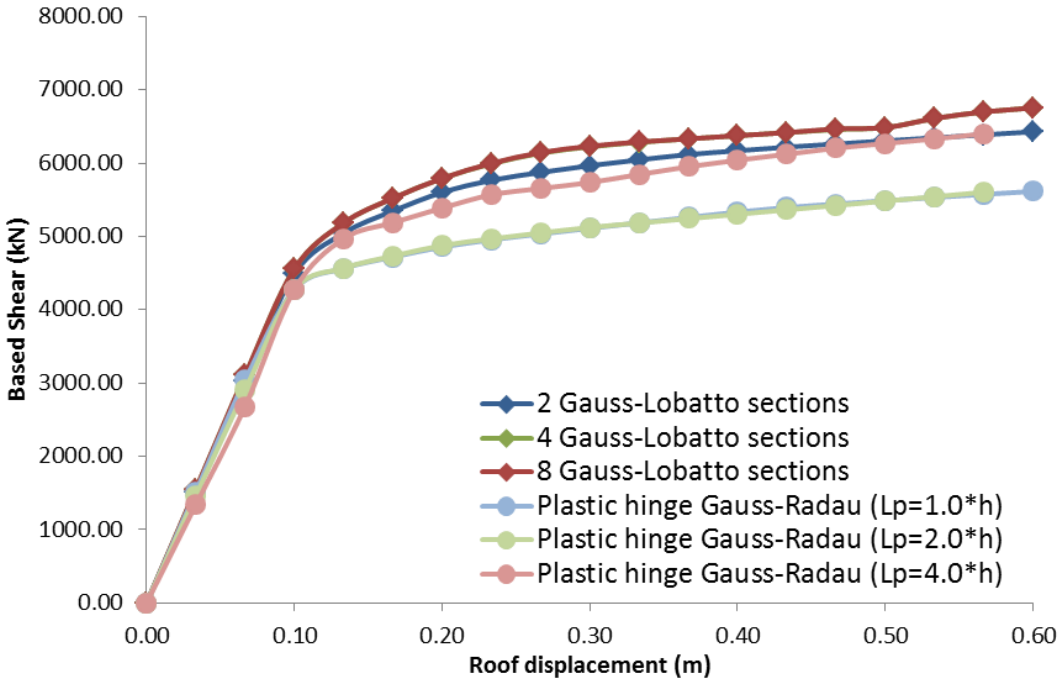

(b)

Fig. 4 Load-displacement response for Gauss-Lobatto integration and Gauss-Radau for the (a) four storey and (b) eight storey steel examples

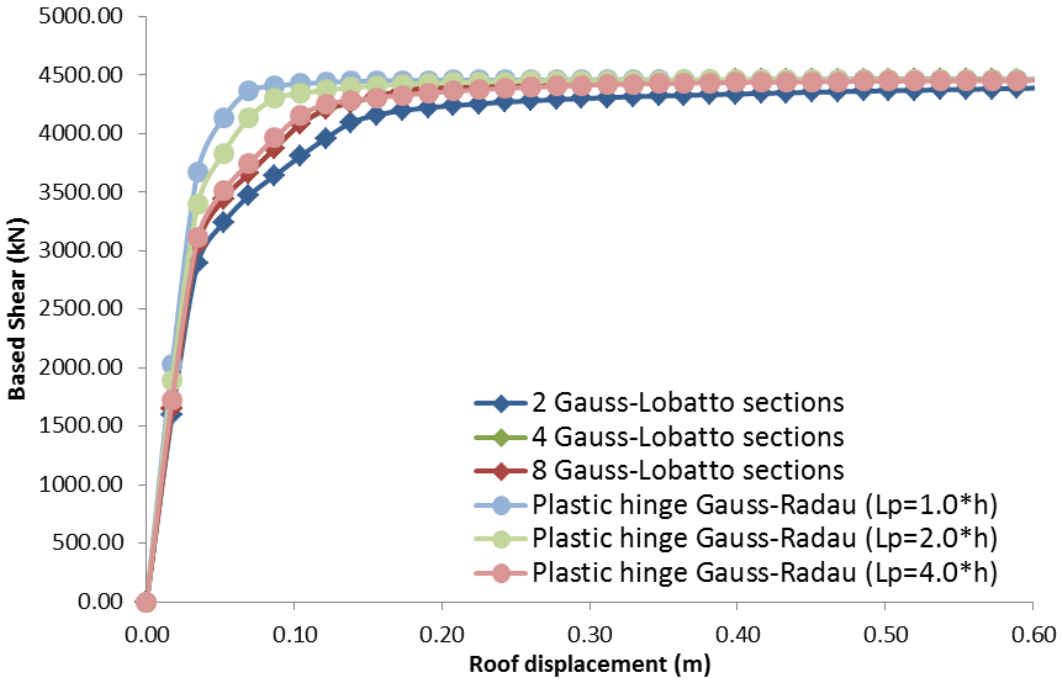

(a)

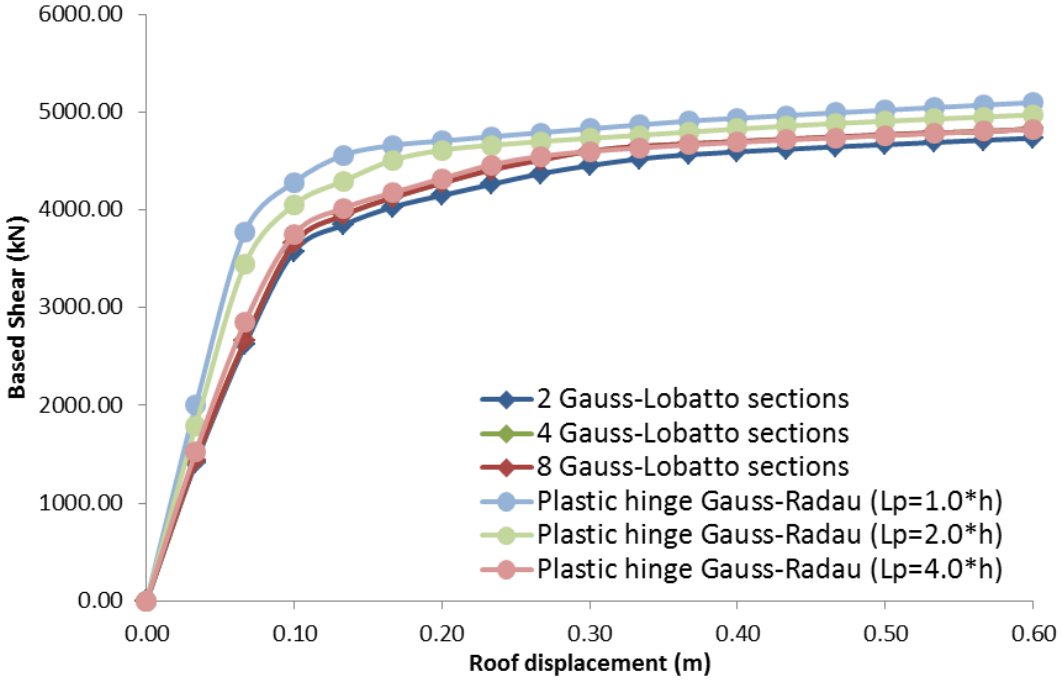

(b)

Fig. 5 Load-displacement response for Gauss-Lobatto integration and Gauss-Radau for the (a) four storey and (b) eight storey steel-reinforced concrete composite examples

the composite sections are considered as independent random variables, while randomness on the material properties is considered for the structural elements only. Furthermore, one random variable is considered for the ground motion excitation, one for the incident angle, one for the damping and one random variable for each floor mass. In order to account for the randomness of the incident angle, the ground motions are applied with a random angle with respect to the structural axes in the range of 0 to 180 degrees. The characteristics of the random variables based on the work by Ellingwood *et al.* (1980), Ellingwood and Galambos (1982) are provided in Table 1, where the mean value of the concrete compressive strength is 12% higher than its nominal value, the mean value of the yield stress for the steel reinforcement is 5% higher than its nominal value and that of the structural steel is 17% higher than its nominal value.

For the purposes of the present investigation six cases are examined where different combinations of random variables are considered into the fragility assessment framework described in Table 2. In the first five cases the force-based beam-column element with fibre modelling was used, in the last case considered *Case 6* stands for the case where the combination of all sources of uncertainty is implemented with the plastic hinges modelling approach. Therefore, the maximum number of random variables considered is: up to 13 for the four storeys steel building, up to 17 for the eight storeys steel building, up to 18 for the four storeys composite building and up to 22 for the eight storeys composite building.

Table 1 Random variables

Random variable		Distribution (PDF)	Mean	CoV
	Earthquake	Uniform	-	-
	Incident angle	Uniform	-	-
Material	f_c (concrete)	Lognormal	22.5 MPa	13%
	E_c (concrete)	Lognormal	3.0×10^7 kN/m²	13%
	f_y (structural steel)	Lognormal	585 MPa	17%
	E_s (structural steel)	Lognormal	2.0×10^8 kN/m²	17%
	b (structural steel)	Lognormal	1%	17%
	$f_{y,r}$ (reinforcement steel)	Lognormal	250 MPa	11%
	$E_{s,r}$ (reinforcement steel)	Lognormal	2.0×10^8 kN/m²	11%
	b_r (reinforcement steel)	Lognormal	1%	11%
	Storey Mass	Normal	180t	10%
	Damping	Normal	4% (steel) 5% (composite)	20%

Table 2 Cases considered

	Random variables
Case 1	Earthquake – incident angle
Case 2	Earthquake – incident angle, material uncertainty
Case 3	Earthquake – incident angle, floor mass uncertainty
Case 4	Earthquake – incident angle, damping uncertainty
Case 5	All sources of uncertainty
Case 6	All sources of uncertainty with the plastic hinges modelling approach

The selection of the proper external loading is not an easy task due to the uncertainties involved in the seismic characteristics. For this reason a rigorous treatment of the seismic loading assumes that the structure is subjected to a set of records that are more likely to occur in the region of its location. In our case a series of 100 seismic records are implemented and they are randomly selected from the list of records given in Tables 3 to 6. These records have been selected from the PEER (2005) strong-motion database with the following features: (i) Events occurred in specific area (longitude -124^o to -115^o, latitude 32^o to 41^o). (ii) Moment magnitude (M) is equal to or greater than 5. (iii) Epicentral distance (R) is smaller than 150 km. In order to account for the randomness of the incident angle, the records are applied with a random angle with respect to the structural axes in the range of 0 to 180 degrees.

6. Fragility assessment of steel and composite buildings

The numerical investigation is composed by two parts. In the first part multicomponent incremental dynamic analysis considering uncertainties is implemented, while in the second part the fragility curves for various limit-states are developed for the steel and steel-RC 3D buildings considered, taking into account the six combinations of the sources of uncertainty. For the purposes of this study multi-component incremental dynamic analysis is used; MIDA is based on the classical incremental dynamic analysis (IDA) that stands for the dynamic analyses performed by increasing the seismic intensity for multiple records.

6.1 Multicomponent incremental dynamic analysis considering uncertainties

The main objective of an MIDA is to define the dynamic capacity curve, corresponding to the relation of the intensity level with the maximum seismic response of the structural system. The intensity level and the seismic response are described through an intensity measure (IM) and an engineering demand parameter, respectively. The MIDA is implemented with the following steps: (i) define the nonlinear FE model required for performing the nonlinear dynamic analyses; (ii) select a suit of natural records, each one represented by its longitudinal and transverse components, which are applied to the structure in order to account for the randomness on the seismic excitation; (iii) select a proper intensity measure and an engineering demand parameter; (iv) employ an appropriate algorithm for selecting the record scaling factor in order to obtain the MIDA curve performing the least required nonlinear dynamic analyses and (v) employ a summarization technique for exploiting the multiple records results.

In MIDA the relation of *IM-EDP* for a single component is defined similarly to the classical incremental dynamic analysis where only one direction of the seismic excitation is considered, i.e. both horizontal components of each record are scaled to a number of intensity levels to encompass the full range of structural behaviour from elastic to yielding that continues to spread, finally leading to global instability. The difference of the MIDA framework from the classical IDA, proposed by Vamvatsikos and Cornell (2002), stems from the fact that for each record a number of representative curves can be defined depending on the incident angle selected, while for the classical IDA only one representative curve is obtained. MIDA is based on the idea of considering variable incident angle for each record, through this implementation randomness both on the seismic excitation and the incident angle are taken into account. A number of available response-based EDPs were discussed and critically evaluated in the past for their applicability in

Table 3 Characteristics of the first set of 22 natural records

Earthquake Station	R[1] (km)	EpiD[2] (km)	Recording Angle log/tran (°)	Duration (sec)	PGA_{log} (g)	PGA_{tran} (g)	Campbell's GEOCODE[3]	Fault rupture[4]
Northridge 1994 (M=6.7)								
Leona Valley #2	37.2	51.88	000/090	32.00	0.09	0.06	A	RN
LA, Baldwin Hills	29.9	28.20	090/360	40.00	0.24	0.17	C	RN
Lake Hughes #1	89.67	93.22	000/090	32.00	0.087	0.077	A	RN
LA, Hollywood Stor FF	114.62	118.26	090/360	40.00	0.231	0.358	A	RN
LA, Centinela St.	31.53	32.72	155/245	30.00	0.465	0.322	A	RN
Anaheim - W Ball Rd	68.62	70.45	220/310	34.99	0.066	0.072	A	RN
Bell Gardens - Jaboneria	44.11	45.26	000/090	34.99	0.049	0.068	A	RN
Loma Prieta 1989 (M=6.9)								
Hollister Diff Array	24.8	45.10	165/255	39.64	0.27	0.28	A	RO
WAHO	17.5	12.56	000/090	24.96	0.37	0.64	C	RO
Halls Valley	30.5	36.31	000/090	39.95	0.13	0.10	B	RO
Agnews State Hospital	24.6	40.12	000/090	40.00	0.17	0.16	A	RO
Anderson Dam (Downstream)	4.4	16.67	270/360	39.61	0.244	0.240	B	RO
Coyote Lake Dam (Downstream)	20.8	30.89	195/285	39.95	0.160	0.179	B	RO
Hollister - South & Pine	27.93	48.24	000/090	60.00	0.371	0.177	A	RO
Imperial Valley 1979 [23:16], (M=6.5)								
Chihuahua	8.4	18.88	012/282	40.00	0.27	0.25	A	SS
Compuertas	15.3	24.43	015/285	36.00	0.19	0.15	A	SS
Plaster City	31.1	54.26	045/135	18.75	0.042	0.057	A	SS
El Centro Array #12	18.85	31.99	140/230	39.00	0.143	0.116	A	SS
El Centro Array #13	22.83	35.95	140/230	39.50	0.117	0.139	A	SS
Bonds Corner	4.01	6.20	140/230	37.60	0.42	0.59	A	SS
Brawley Airport	10.57	43.15	225/315	37.82	0.15	0.16	A	SS
Calexico Fire Station	11.56	17.65	225/315	37.80	0.19	0.27	A	SS

[1]Campbell's R Distance
[2]Distance from the recording site to epicentre
[3]Campbell's site classification: A (Firm Soil), B (Very Firm Soil), C (Soft Rock), D (Firm Rock), E (Shallow Soils)
[4]Fault rupture mechanism: SS (Strike Slip), N (Normal), RN (Reverse-Normal), RO (Reverse-Oblique), NO (Normal- Oblique)

Table 4 Characteristics of the second set of 30 natural records

Earthquake Station	R[1] (km)	EpiD[2] (km)	Recording Angle log/tran (°)	Duration (sec)	PGA_{log} (g)	PGA_{tran} (g)	Campbell's GEOCODE[3]	Fault rupture[4]
Superstition Hills 1987 (B) (M=6.7)								
El Centro Imp. Co Cent	18.5	35.83	000/090	40.00	0.36	0.26	A	SS
Wildlife Liquefaction Array	24.1	29.41	090/360	44.00	0.18	0.21	A	SS
Parachute Test Site	3.53	15.99	225/315	22.31	0.46	0.38	A	SS
Plaster City	22.50	25.98	045/135	22.14	0.19	0.12	A	SS
Brawley Airport	17.37	29.91	225/315	21.97	0.16	0.12	A	SS
Calipatria Fire Station	27.21	31.62	225/315	22.11	0.25	0.18	A	SS
Kornbloom Road	18.79	19.28	270/360	21.98	0.12	0.14	A	SS
Poe Road	11.67	11.20	270/360	22.30	0.30	0.45	A	SS
Salton Sea Wildlife Refuge	26.11	26.48	225/315	21.89	0.17	0.12	A	SS
Superstition Mtn Camera	6.56	7.50	045/135	22.21	0.68	0.89	D	SS
Westmorland Fire Sta	13.47	19.51	090/180	40.00	0.17	0.21	A	SS
San Fernando 1971 (M=6.6)								
LA, Hollywood Stor. Lot	25.9	39.49	090/180	28.00	0.21	0.17	A	RN
Pasadena - CIT Athenaeum	27.16	42.75	000/090	28.49	0.11	0.09	B	RN
LB - Terminal Island	61.82	76.38	249/339	79.98	0.013	0.011	A	RN
San Onofre - So Cal Edison	126.78	142.62	033/303	23.00	0.029	0.029	C	RN
Castaic - Old Ridge Route	22.63	25.36	021/291	30.00	0.17	0.27	C	RN
Cedar Springs, Allen Ranch	89.72	100.39	095/185	14.66	0.009	0.015	D	RN
Lake Hughes #1	27.40	26.10	021/111	30.00	0.098	0.11	A	RN
Santa Anita Dam	31.41	45.86	003/273	29.66	0.062	0.151	D	RN
Coalinga 1983/05/02 [23:42] (M=6.4)								
Cantua Creek School	24.02	30.06	270/360	40.00	0.227	0.281	A	RN
Parkfield - Cholame 2WA	44.72	55.67	000/090	40.00	0.109	0.114	A	RN
Parkfield - Cholame 5W	48.70	59.67	270/360	40.00	0.147	0.131	A	RN
Parkfield - Fault Zone 1	41.99	52.86	000/090	40.00	0.194	0.111	A	RN
Parkfield - Fault Zone 14	29.48	38.54	000/090	40.00	0.282	0.274	A	RN
Parkfield - Gold Hill 3W	39.12	49.47	000/090	40.00	0.137	0.122	B	RN
Parkfield - Stone Corral 3E	34.00	44.66	000/090	24.00	0.151	0.106	C	RN
Pleasant Valley P.P. - yard	8.41	9.98	045/135	39.97	0.592	0.551	A	RN
Parkfield - Fault Zone 4	34.59	44.83	000/090	40.00	0.067	0.12	C	RN
Parkfield - Vineyard Cany 2W	30.35	38.47	000/090	30.00	0.073	0.083	C	RN
Slack Canyon	27.46	33.52	045/315	30.00	0.153	0.166	D	RN

Table 5 Characteristics of the third set of 23 natural records

Earthquake Station	R[1] (km)	EpiD[2] (km)	Recording Angle log/tran (°)	Duration (sec)	PGA_{log} (g)	PGA_{tran} (g)	Campbell's GEOCODE[3]	Fault rupture[4]
Whittier Narrows 1987/10/01 (M=6.0)								
Pasadena - CIT Athenaeum	17.24	10.64	180/270	32.00	0.174	0.101	B	RO
Alhambra - Fremont School	14.66	6.77	180/270	40.00	0.333	0.414	B	RO
LA - Hollywood Stor FF	24.08	24.21	000/090	40.00	0.221	0.124	A	RO
Altadena - Eaton Canyon	19.52	14.28	000/090	40.00	0.299	0.151	A	RO
Beverly Hills - 12520 Mulhol	29.90	31.09	032/122	32.22	0.089	0.138	C	RO
Brea Dam (Downstream)	23.99	22.72	040/130	30.00	0.163	0.313	A	RO
Glendale - Las Palmas	22.82	21.73	177/267	31.50	0.296	0.166	A	RO
Riverside Airport	55.48	59.59	180/270	39.99	0.05	0.047	A	RO
Chalfant Valley 1986/07/20 (M=5.9)								
Benton	21.92	31.25	270/360	32.00	0.061	0.052	A	SS
Bishop - Paradise Lodge	18.31	15.42	070/160	39.95	0.046	0.095	C	SS
Bishop - LADWP South St	17.17	20.27	180/270	39.93	0.129	0.094	A	SS
Lake Crowley - Shehorn Res.	22.08	16.59	009/099	40.00	0.051	0.031	A	SS
Zack Brothers Ranch	7.58	14.33	270/360	39.87	0.285	0.207	A	
Coyote Lake 1979 (M=5.7)								
Gilroy Array #1	10.67	12.56	230/320	26.84	0.103	0.132	D	SS
Coyote Lake Dam (SW Abut)	6.13	7.95	160/250	28.82	0.157	0.279	D	SS
Gilroy Array #2	9.02	10.94	050/140	26.86	0.211	.339	A	SS
Gilroy Array #6	3.11	4.37	230/320	27.10	0.434	0.316	C	SS
San Juan Bautista	19.70	23.24	213/303	28.46	0.108	0.107	B	SS
Halls Valley	33.83	36.29	150/240	40.00	0.039	0.050	B	SS
SJB Overpass, Bent 3 g.l.	20.67	23.91	067/337	26.83	0.124	0.097	D	SS
Overpass, Bent 5 g.l.	20.67	23.91	067/337	26.83	0.114	0.073	D	SS
Gilroy Array #3	7.42	9.59	050/140	26.80	0.228	0.272	A	SS
Gilroy Array #4	5.70	7.67	270/360	27.18	0.271	0.248	A	SS

Table 6 Characteristics of the fourth set of 25 natural records

Earthquake Station	R[1] (km)	EpiD[2] (km)	Recording Angle log/tran (°)	Duration (sec)	PGA_{log} (g)	PGA_{tran} (g)	Campbell's GEOCODE[3]	Fault rupture[4]
Cape Mendocino 1992 (M=7.1)								
Cape Mendocino	6.96	10.36	000/090	30.00	1.497	1.039	D	RN
Eureka - Myrtle & West	41.97	53.34	000/090	44.00	0.154	0.178	B	RN
Fortuna - Fortuna Blvd	19.95	29.55	000/090	44.00	0.116	0.114	A	RN
Petrolia	8.18	4.51	000/090	36.00	0.590	0.662	A	RN
Rio Dell Overpass - FF	14.33	22.64	270/360	36.00	0.385	0.549	A	RN
Shelter Cove Airport	28.78	36.28	000/090	36.00	0.229	0.189	E	RN
Westmorland 1981 (M=5.8)								
Brawley Airport	15.57	15.71	225/315	28.41	0.169	0.171	A	SS
Niland Fire Station	15.45	18.45	000/090	40.00	0.105	0.176	A	SS
Parachute Test Site	16.81	20.47	225/315	40.00	0.242	0.155	A	SS
Superstition Mtn Camera	19.50	25.02	045/135	28.36	0.071	0.116	D	SS
Westmorland Fire Sta	6.87	7.02	090/180	40.00	0.368	0.496	A	SS
Salton Sea Wildlife Ref	8.15	8.62	225/315	28.75	0.199	0.176	A	SS
Landers 1992 (M=7.3)								
Desert Hot Springs	21.98	27.33	000/090	50.00	0.171	0.154	A	SS
Amboy	69.17	75.20	000/090	50.00	0.115	0.146	E	SS
Lucerne	3.71	44.02	000/090	48.13	0.721	0.785	D	SS
Hemet Fire Station	68.72	72.51	000/090	56.00	0.081	0.097	A	SS
Indio - Coachella Canal	54.34	59.68	000/090	60.00	0.104	0.109	A	SS
Joshua Tree	11.43	13.67	000/090	44.00	0.274	0.284	A	SS
Morongo Valley	17.58	21.29	000/090	70.00	0.14	0.188	A	SS
North Palm Springs	27.01	32.26	000/090	70.00	0.134	0.136	A	SS
Palm Springs Airport	36.27	41.87	000/090	60.00	0.089	0.076	A	SS
Puerta La Cruz	94.53	100.12	000/090	65.00	0.044	0.047	E	SS
Riverside Airport	96.05	97.13	180/270	50.00	0.041	0.043	A	SS
Arcadia - Campus Dr	135.26	147.53	009/279	59.08	0.051	0.046	A	SS
Baldwin Park - N Holly	131.95	142.08	180/270	34.30	0.026	0.028	A	SS

seismic damage evaluation. In the current work the maximum interstorey drift θ_{max} was chosen, because there is an established relation between interstorey drift value with performance-oriented descriptions, such as immediate occupancy, life safety and collapse prevention.

In order to consider additional sources of randomness the procedure proposed by Dolsek (2009) is implemented into the MIDA framework. Therefore, N_{sim} samples of record incident angle-random variables are generated by means of the Latin hypercube sampling (LHS) method, IDA is conducted for each sample and the representative dynamic capacity curve for the sample in question is developed. LHS is a strategy for generating random sample points ensuring that all portions of the random space are properly represented. In LHS a full stratification of the sampled distribution with a random selection inside each stratum is performed and the sample values are randomly shuffled among different variables. A Latin hypercube sample is constructed by dividing the range of each of the K random variables into N_{sim} non-overlapping segments of equal marginal probability. Thus, the whole parameter space, consisting of K parameters, is partitioned into N_{sim}^{K} cells. A single value is selected randomly from each interval, producing N_{sim} sample values for each random variable. The values are randomly matched to create N_{sim} sets, from the N_{sim}^{K} space with respect to the density of each interval, for the N_{sim} simulation runs. In order to implement the proposed procedure the number of simulations (N_{sim}) should be a whole multiplier of the number of records M_{rec}. Therefore, the samples of incident angle-random variables combined with each record m = 1, 2,..., M_{rec} is equal to $n = N_{sim}/M_{rec}$, hence for each record n samples of the incident angle-random variables are generated by means of LHS. A schematic representation of the proposed procedure can be seen in Fig. 6, where the MIDA is implemented over a sample of record-two random variables generated using LHS.

For the needs of the first part of the study, the four buildings are subjected to an ensemble of M_{rec} = 100 natural records selected in the area of San Diego in California, while n = 50 samples of record-random variables generated using LHS are generated, thus $N_{sim} = n \times M_{rec}$ = 5,000 samples are used, for instance in *Case 2* for each record 50 random incident angles are generated. The increment steps have been chosen in a way to optimize the number of analyses, thus every MIDA study is performed for N_{ISt} 10 specific incremental steps (0.10g, 0.19g, 0.26g, 0.30g, 0.44g, 0.55g, 0.82g, 0.95g, 1.12g and 1.20g). The results of the 4 buildings × N_{sim} samples × N_{ISt} steps = 200,000 nonlinear time-history analyses are post-processed in order to create a response databank with the

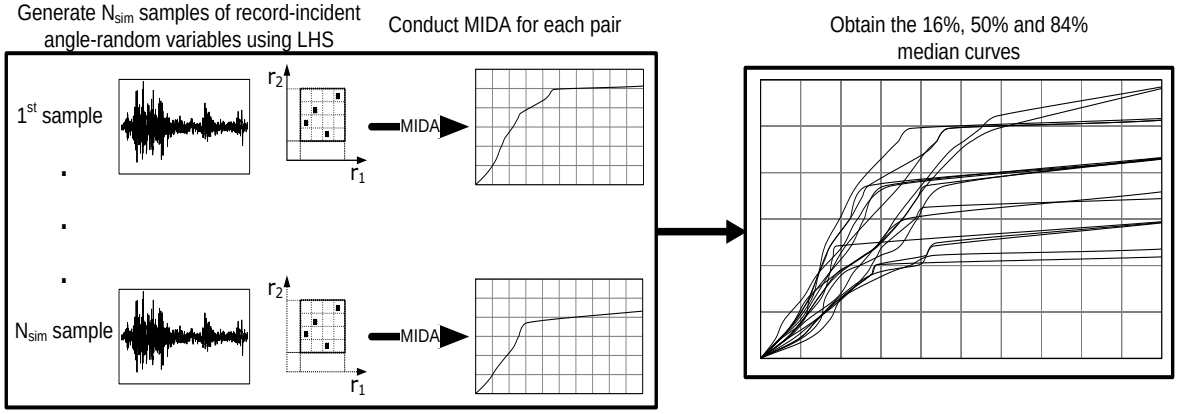

Fig. 6 MIDA framework considering uncertainties

maximum interstorey drift ratio along the height of the buildings. The contribution of the sources of uncertainty is represented with the distribution of the drift values for three hazard levels selected from the MIDA curves (30%, 10% and 2% exceedance in 50 years), that are depicted in Fig. 7 to Fig. 10 for the four test examples, respectively. Comparing the bottom and top values of the blue boxes that define the 25% and 75% percentiles, the red line that defines the median value and the minimum and maximum values of the drift values defined with the black lines, it can be seen that significant variances are noticed. For the 4 storey steel building compared to *Case 1* the difference is magnified for *Case 4*, *Case 5* and *Case 6*. For the 8 storey steel building compared to *Case 1* the difference is magnified for *Case 2* and *Case 4*. For the 4 storey steel-RC composite building compared to *Case 1* the difference is magnified for *Case 2* and *Case 4*. While For the 8 storey steel-RC composite building compared to *Case 1* the difference is reduced for all cases except for *Case 2*. Furthermore, as it can be seen in Fig. 7, although there are additional sources of uncertainty, in the four storey steel test example, for *Case 3* the dispersion is lower than in *Case 1*. The same behaviour can be observed also by looking other *Cases* for the other structures. In addition, it is interesting to observe that often there is not consistency of the results among the different structures considered. For example, while *Case 3* is that one with less dispersion for the four storey steel structure, in the eight storey steel structure is probably that one that is characterized by the higher dispersion. This is because, the effect of randomness is structure dependent.

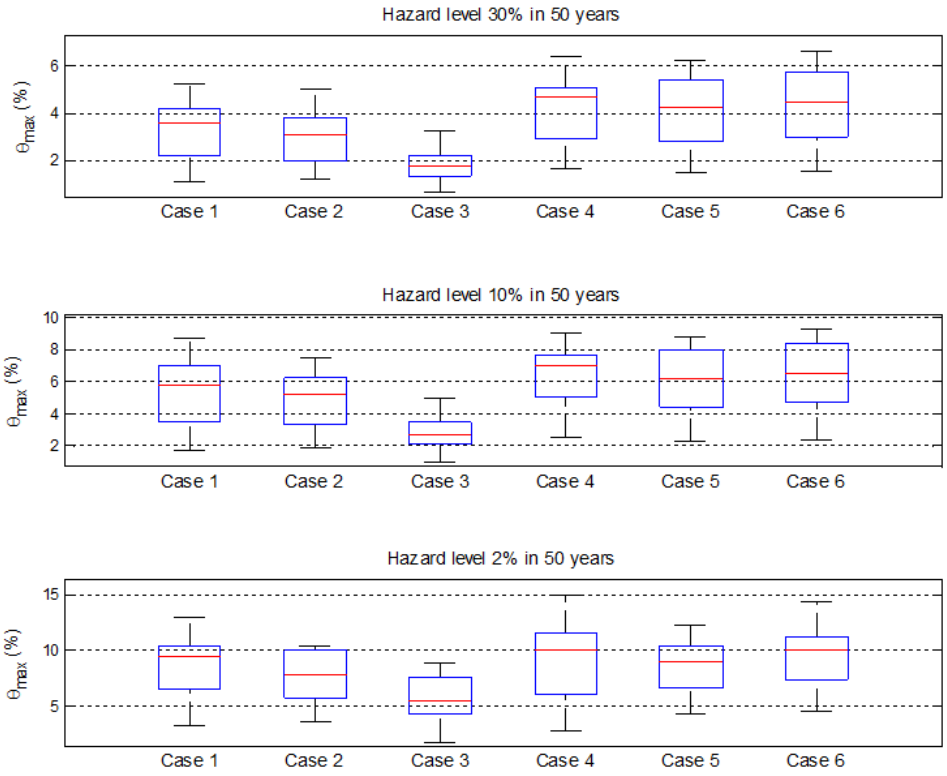

Fig. 7 Four storey steel test example - boxplots with the contribution of sources of uncertainty on the drift values

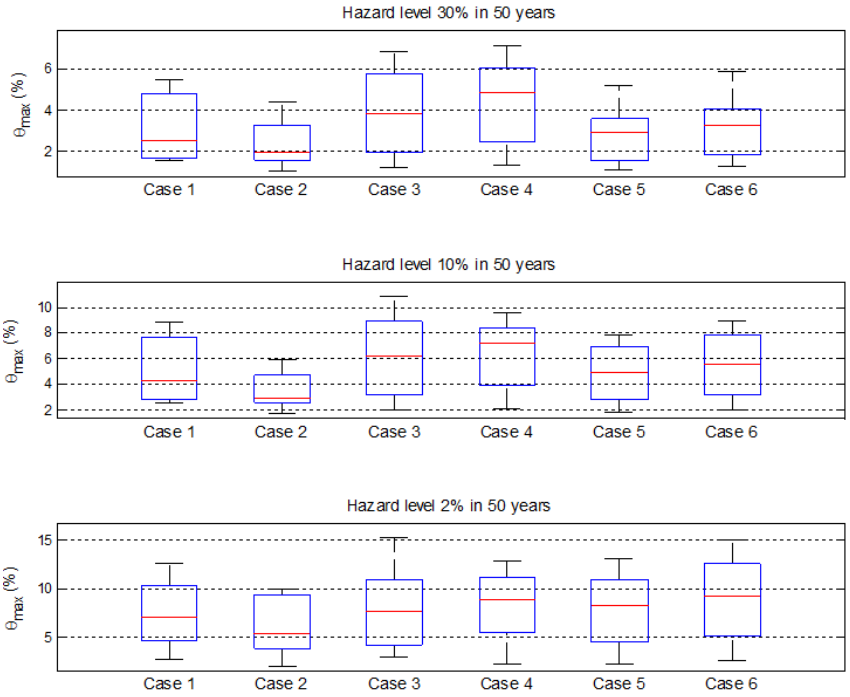

Fig. 8 Eight storey steel test example - boxplots with the contribution of sources of uncertainty on the drift values

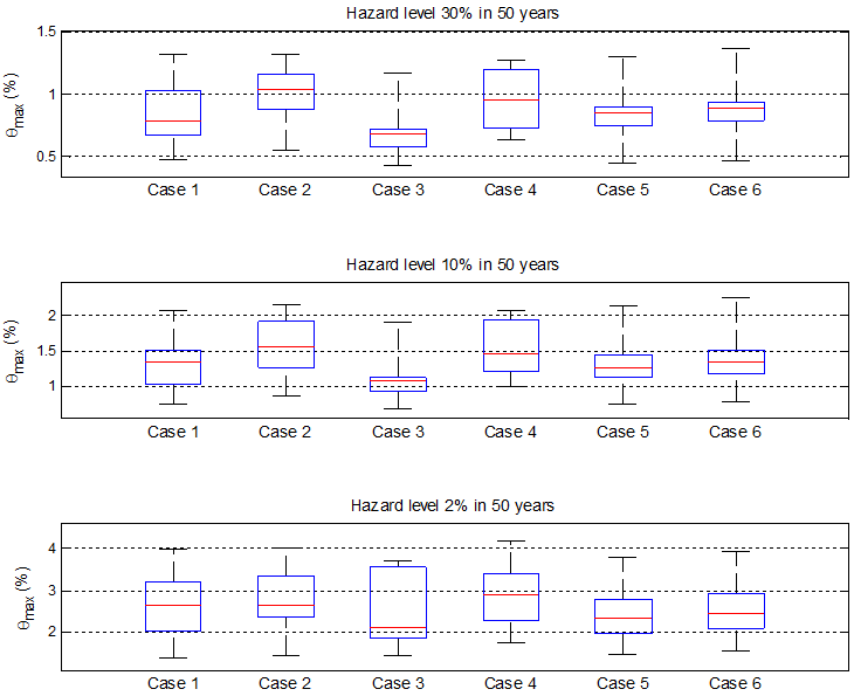

Fig. 9 Four storey steel-RC composite test example - boxplots with the contribution of sources of uncertainty on the drift values

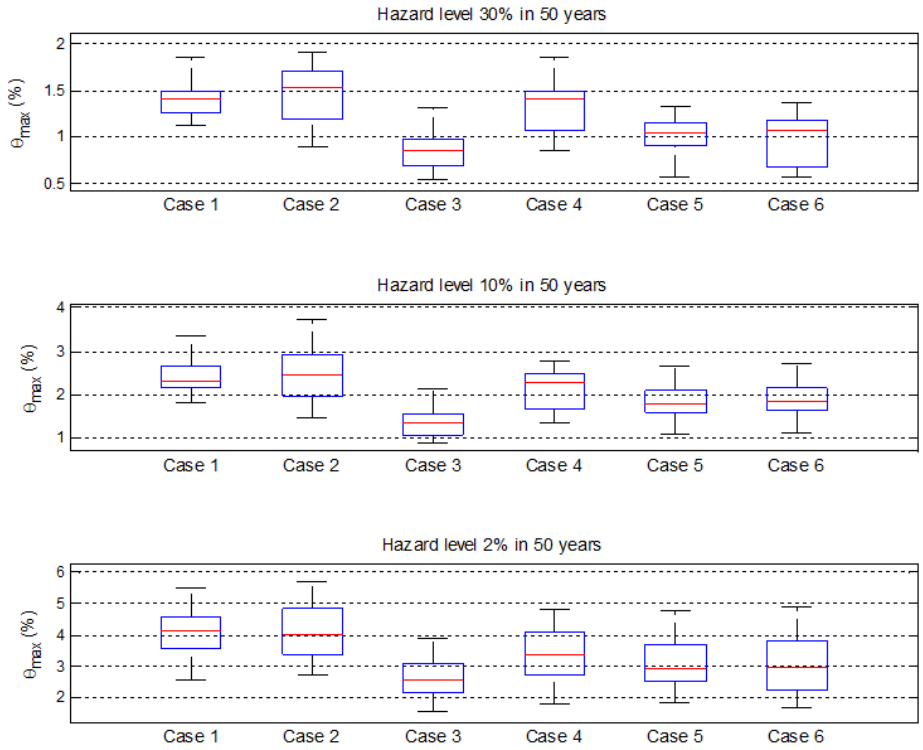

Fig. 10 Eight storey steel-RC composite test example - boxplots with the contribution of sources of uncertainty on the drift values

6.2 Fragility assessment

Four limit-state fragility curves are obtained for each one of the four buildings of Fig. 1. The limit-states considered are defined by means of maximum drift values and cover the whole range of structural damage from slight damage to collapse for mid and high rise steel and steel-RC composite buildings as defined by HAZUS (2003). The following $\theta_{\max}$ values are used for each of the four limit-states: (2/3)×(0.5, 1.0, 3.0 and 8.0) for the four storey steel and steel-RC composite buildings and (1/2)×(0.5, 1.0, 3.0 and 8.0) for the eight storey ones.

The fragility analysis based on the MIDA procedure, requires dynamic analyses for different intensity levels to be carried out for a sufficiently large number of ground motions in order to perform a statistical evaluation of the results (in this study M_{rec}=100 natural records are used). Statistical information necessary to understand and quantify the behaviour of structural systems can be presented in different formats depending upon the objective. For instance, if the issue is loss assessment, for which it is important to evaluate the distribution, mean value and/or dispersion of an EDP given the IM, the "horizontal" statistics format is considered the most appropriate (Fig. 11). However, if the issue is conceptual design or fragility analysis, where the designer wants to find the global strength required to limit the value of an EDP to a certain quality, then "vertical" statistics are the most suitable (Fig. 11). "Vertical" statistics are also used to quantify the ground motion intensity at which a system approaches a certain limit-state (Medina and Krawinkler 2004). The terms "horizontal" and "vertical" presuppose that EDPs are plotted on the horizontal axis and

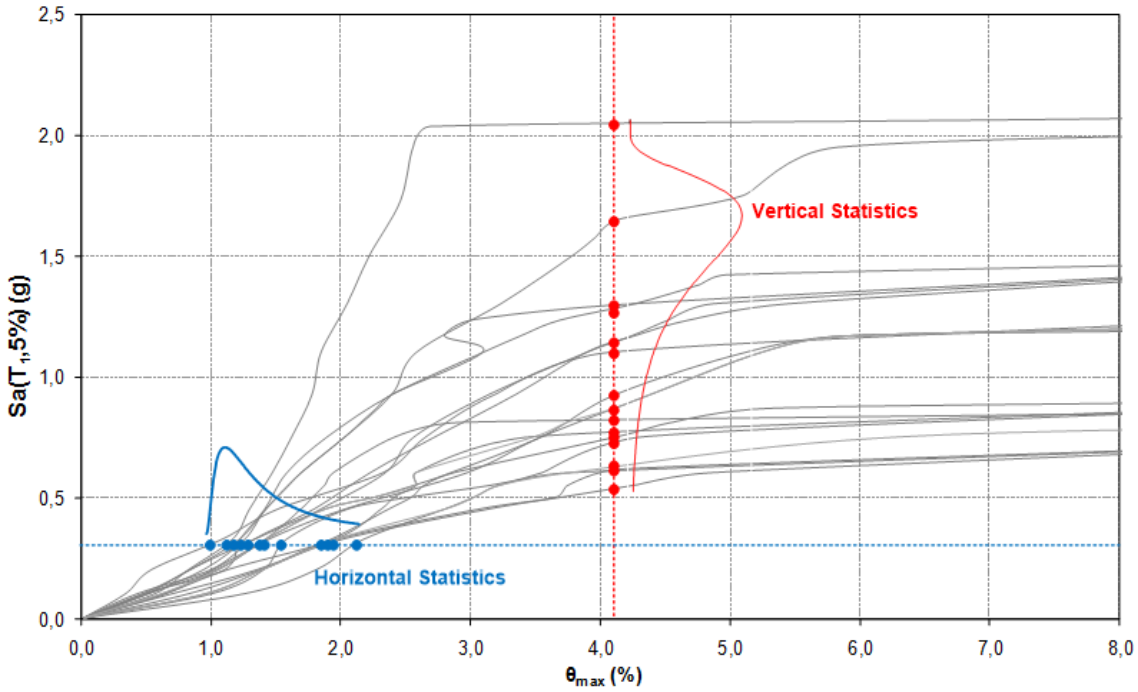

Fig. 11 IDA curve-"vertical" and "horizontal" statistics

IMs on the vertical axis. Since the work of this study is concerned with fragility analysis, the focus is on "vertical" statistics in order to calculate, via optimization, the two parameters μ and β of Eq. (4) that maximize ln(L). Since four limit-state fragilities are developed for each building, eight parameters are defined solving this maximization problem. For this purpose DE method is implemented using the following parameters: population size NP = 100, probability CR = 0.90, mutation constant F = 0.47 and control variable λ = 0.2, based on the parametric study by Pedersen (2010).

Since the end product of analysis would be to compute the long-term probability that a certain limit state will be exceeded in a building located at a certain site, it is essential to evaluate the influence of the sources of uncertainty in terms of the mean annual frequencies (MAF) of limit-state exceedance. Tables 7 to 10 shows the mean annual frequencies obtained after

Table 7 Four storey steel example-Mean annual frequencies of limit-state exceedance

	$\theta_{max} \geq 0.33\%$	$\theta_{max} \geq 0.67\%$	$\theta_{max} \geq 2.00\%$	$\theta_{max} \geq 5.33\%$
Case 1	1.13E-02	7.87E-03	2.97E-03	7.59E-04
Case 2	8.99E-03	6.15E-03	2.54E-03	8.16E-04
Case 3	5.67E-03	3.28E-03	9.94E-04	2.36E-04
Case 4	1.05E-02	7.46E-03	3.16E-03	9.83E-04
Case 5	7.31E-03	4.80E-03	1.90E-03	6.11E-04
Case 6	7.53E-03	4.99E-03	1.93E-03	2.76E-04

Table 8 Eight storey steel example-Mean annual frequencies of limit-state exceedance

	$\theta_{max} \geq 0.25\%$	$\theta_{max} \geq 0.50\%$	$\theta_{max} \geq 1.50\%$	$\theta_{max} \geq 4.00\%$
Case 1	1.37E-02	1.11E-02	6.27E-03	2.77E-03
Case 2	1.51E-02	1.32E-02	7.82E-03	3.18E-03
Case 3	1.52E-02	1.35E-02	8.49E-03	3.82E-03
Case 4	1.37E-02	1.12E-02	6.66E-03	3.23E-03
Case 5	1.50E-02	1.31E-02	7.89E-03	3.32E-03
Case 6	1.52E-02	1.35E-02	8.65E-03	4.15E-03

Table 9 Four storey composite example-Mean annual frequencies of limit-state exceedance

	$\theta_{max} \geq 0.33\%$	$\theta_{max} \geq 0.67\%$	$\theta_{max} \geq 2.00\%$	$\theta_{max} \geq 5.33\%$
Case 1	1.89E-03	5.06E-04	2.75E-05	1.12E-06
Case 2	2.47E-03	8.00E-04	6.28E-05	3.51E-06
Case 3	2.08E-03	6.94E-04	5.93E-05	2.95E-06
Case 4	1.89E-03	6.59E-04	8.86E-05	1.35E-05
Case 5	1.95E-03	7.15E-04	7.40E-05	4.11E-06
Case 6	2.06E-03	7.75E-04	8.52E-05	5.56E-06

Table 10 Eight storey composite example-Mean annual frequencies of limit-state exceedance

	$\theta_{max} \geq 0.25\%$	$\theta_{max} \geq 0.50\%$	$\theta_{max} \geq 1.50\%$	$\theta_{max} \geq 4.00\%$
Case 1	6.33E-03	3.37E-03	9.48E-04	2.87E-04
Case 2	7.02E-03	4.03E-03	1.31E-03	3.45E-04
Case 3	5.74E-03	2.78E-03	6.56E-04	1.25E-04
Case 4	8.59E-03	4.53E-03	8.11E-04	5.96E-05
Case 5	6.73E-03	3.34E-03	7.33E-04	1.07E-04
Case 6	6.90E-03	3.46E-03	7.72E-04	2.53E-04

the fragility curves with the hazard curve of Fig. 12, as suggested by Eq. (1). In order to calculate the MAF values of Tables 7 to 10, the hazard curve of Fig. 12 is modified for each structure in order to account for the variation of the structural period. The region under examination was chosen to be the city of San Diego, California (Latitude (N) 32.7^o, Longitude (W) -117.2^o), thus the hazard curve of Fig. 12 corresponds to this area. For the four storey steel building compared to *Case* 5 the differences between MAF is up to 60% for some of the limit-states. In particular the differences of *Case* 6 are negligible for first three limit-states and up to 55% for the collapse limit-state, *Case 1*, *Case 2* and *Case 4* overestimate MAF for all limit-states, while *Case 3* underestimates the limit-states. For the eight storey steel building compared to *Case 5* the differences between MAF is up to 20% for some of the limit-states. In particular the differences of *Case 2*, *Case 3* and *Case 6* are negligible for three first limit-states and up to 25% for the collapse limit-state; while *Case 1* and *Case 2* overestimate MAF for all limit-states. For the four storey steel-RC building compared to *Case 5* the differences between MAF is up to 60% for some of the limit-states. In particular the differences of *Case 6* are negligible for three first limit-states and up

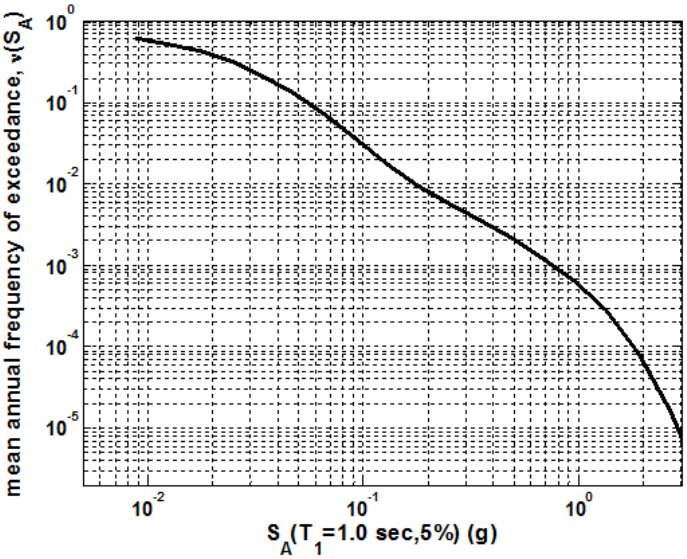

Fig. 11 IDA curve-"vertical" and "horizontal" statistics

to 35% for the collapse limit-state; *Case 2* and *Case 4* overestimate MAF for some of the limit-states and underestimate some others, while *Case 1* and *Case 3* underestimates MAF of the limit-states. For the eight storey steel-RC composite building the differences between MAF is up to 200% for all limit-states. In particular the differences of *Case 6* are negligible for first three limit-states and up to 135% for the collapse limit-state, *Case 1*, *Case 3* and *Case 4* overestimate MAF for some of the limit-states and underestimate some others, while *Case 2* overestimates the limit-states.

7. Conclusions

In this work fragility curves associated with different limit-states of steel and steel-reinforced concrete composite buildings are developed, considering the influence of various sources of uncertainty. In particular randomness on the seismic demand and incident angle along with the uncertainty on the material properties, the floor mass and the structural damping properties are considered. Furthermore, the contribution of the modelling approach (fibre versus plastic hinges) is also examined. The drift limit-state fragility curves cover the whole range of structural damage from serviceability, to life safety and finally to the onset of collapse. For this purpose two steel and two steel-reinforced concrete composite 3D buildings are considered with four and eight storeys.

In order to perform fragility analysis based on the incremental dynamic analysis methodology, dynamic analyses for different intensity levels need to be carried out for a number of ground motions sufficiently large to perform statistical evaluation of the results. Statistical information necessary to understand and quantify the behaviour of structural systems can be presented in different formats (horizontal or vertical statistics) depending upon the objective. In the case of fragility analysis where the designer desires to find seismic demand given the structural capacity represented by the value of an engineering demand parameter, "vertical" statistics are required. For

the calculation of the optimum values of the two characteristic parameters of the fragility curve function the Differential Evolution optimization algorithm is implemented.

The distribution of the drift values varies significantly both in terms of 25, 50 and 75 percentiles but also with respect to the maximum and minimum values. As it was observed, although there are additional sources of uncertainty for *Case 3* the dispersion is lower than in *Case 1*. In addition, it is interesting to observe that often there is not consistency of the results among the different structures considered. This is because, the effect of randomness is structure dependent. Furthermore, comparing the six combinations of the sources of uncertainty with reference to the mean annual frequency of exceedance it should be noted that disregarding the cumulative effect of all sources may lead to significant overestimation or underestimation.

For the test examples considered in this study, material and floor mass were found to be very significant sources of uncertainty. As it was observed from the results attained, if both sources are ignored (i.e. *Case 4*) significant differences with respect to mean annual frequencies are obtained. Furthermore, it should be noticed that the mean annual frequencies obtained for the four structures differ in a rather systematic way for the first three limit-states while deviation from this rule is detected for the four storey composite test example in the case of the higher limit-state (i.e. $\theta_{\max} \geq$ 5.33% limit-state). While, comparing *Cases 5* and *6*, where all sources of uncertainty are considered and vary only with respect to modelling, it can be observed from the results that they differ for the higher limit-states only while for the lower ones these two cases provide quit similar results. In addition, an observation that might not be intuitive from engineering knowledge is that mean annual frequencies might reduce when all sources are considered (i.e. *Cases 5* and *6*).

Acknowledgments

This work has been supported by the European Research Council Advanced Grant "MASTER– Mastering the computational challenges in numerical modeling and optimum design of CNT reinforced composites" (ERC-2011-ADG_20110209).

References

ANSI/AISC 341-10 (2010), *Seismic provisions for structural steel buildings*, AISC, Chicago, Illinois, June.

Aslani, H. and Miranda, E. (2005), "Probability-based seismic response analysis", *Eng. Struct.*, **27**(8), 1151-1163.

Aygün, B., Duẽas-Osorio, L., Padgett, J.E. and Desroches, R. (2011), "Efficient longitudinal seismic fragility assessment of a multispan continuous steel bridge on liquefiable soils", *J. Bridge Eng.*, **16**(1), 93-107.

Celik, O.C. and Ellingwood, B.R. (2010), "Seismic fragilities for non-ductile reinforced concrete frames - role of aleatoric and epistemic uncertainties", *Struct. Safe.*, **32**(1), 1-12.

Dolsek, M. (2009), "Incremental dynamic analysis with consideration of modelling uncertainties", *Earthq. Eng. Struct. Dyn.*, **38**(6), 805-825.

Eleftheriadou, A.K. and Karabinis, A.I. (2012), "Seismic vulnerability assessment of buildings based on damage data after a near field earthquake (7 September 1999 Athens - Greece)", *Earthq. Struct.*, **3**(2), 117-140.

Ellingwood, B.R. (2001), "Earthquake risk assessment of building structures", *Reliab. Eng. Syst. Safe.*, **74**(3), 251-262.

Ellingwood, B.R. and Galambos, T.V. (1982), "Probability-based criteria for structural design", *Struct. Saf.*,

1(1), 15-26.
Ellingwood, B.R., Galambos, T.V., MacGregor, J.G. and Cornell, C.A. (1980), *Development of a probability-based load criterion for American National Standard A58*, National Bureau of Standards, Washington DC.
Fragiadakis, M. and Lagaros, N.D. (2011), "An overview to structural seismic design optimisation frameworks", *Comput. Struct.*, **89**(11-12), 1155-1165.
Fragiadakis, M. and Papadrakakis, M. (2008), "Modelling, analysis and reliability of seismically excited structures: computational issues", *Int. J. Comput. Method.*, **5**(4), 483-511.
Gardoni, P., Mosalam, K.M. and Der Kiureghian, A. (2003), "Probabilistic seismic demand models and fragility estimates for RC bridges", *J. Earthq. Eng.*, **7**(1), 79-106.
Hauke, B., Gudel, M. and Obiala, R. (2008), "Experimental study of composite column-wall systems subjected to combined loading conditions", *EUROSTEEL 2008*, 3-5 September 2008, ECCS European Convention for Constructional Steelwork.
HAZUS-MH MR1 (2003), *Multi-hazard loss estimation methodology earthquake model*, FEMA-National Institute of Building Sciences, Washington DC.
Jeong, S.H. and Elnashai, A.S. (2007), "Probabilistic fragility analysis parameterized by fundamental response quantities", *Eng. Struct.*, **29**(6), 1238-1251.
Kappos, A.J., Panagopoulos, G., Panagiotopoulos, C. and Penelis, G. (2006), "A hybrid method for the vulnerability assessment of R/C and URM buildings", *Bull. Earthq. Eng.*, **4**(4), 391-413.
Kennedy, R.P,. Cornell, C.A., Campbell, R.D., Kaplan, S. and Perla, H.F. (1980), "Probabilistic seismic safety study of an existing nuclear power plant", *Nucl. Eng. Des.*, **59**(2), 315-338.
Kent, D.C. and Park, R. (1971), "Flexural members with confined concrete", *J. Struct. Div.*, **97**(7), 1969-1990.
Kim, J.H., Choi, I.K. and Park, J.H. (2011), "Uncertainty analysis of system fragility for seismic safety evaluation of NPP", *Nucl. Eng. Des.*, **241**(7), 2570-2579.
Kircher, C.A., Nassar, A.A., Kustu, O. and Holmes, W.T. (1997), "Development of building damage functions for earthquake loss estimation", *Earthq. Spectra*, **13**(4), 663-682.
Lagaros, N.D. (2008), "Probabilistic fragility analysis of RC buildings designed with different rules", *Earthq. Eng. Eng. Vib.*, **7**(1), 45-56.
Lagaros, N.D. (2010), "Multicomponent incremental dynamic analysis considering variable incident angle", *Struct. Infr. Eng.*, **6**(1-2), 77-94.
Lagaros, N.D. and Karlaftis, M.G. (2011), "A critical assessment of metaheuristics for scheduling emergency infrastructure inspections", *Swarm Evolut. Computat.*, **1**(3), 147-163.
Lagaros, N.D. and Papadrakakis, M. (2012), "Applied soft computing for optimum design of structures", *Struct. Multidiscip. O.*, **45**, 787-799.
Liel, A.B., Haselton, C.B., Deierlein, G.G. and Baker, J.W. (2009), "Incorporating modelling uncertainties in the assessment of seismic collapse risk of buildings", *Struct. Safe.*, **31**(2), 197-211.
McKenna, F. and Fenves, G.L. (2001), *The OpenSees command language manual - Version 1.2.*, Pacific Earthquake Engineering Research Centre, University of California, Berkeley.
Medina, R.A. and Krawinkler, H. (2004), "Seismic demands for nondeteriorating frame structures and their dependence on ground motions", PEER Report 2003/15, Pacific Earthquake Engineering Research Center, College of Engineering, University of California, Berkeley, CA.
Menegotto, M. and Pinto, P.E. (1973), "Method of analysis for cyclically loaded reinforced concrete plane frames including changes in geometry and non-elastic behaviour of elements under combined normal force and bending", *Proceedings, IABSE Symposium on Resistance and Ultimate Deformability of Structures Acted on by Well Defined Repeated Loads*, 15-22.
Mitropoulou, C.C., Lagaros, N.D. and Papadrakakis, M. (2010), "Building design based on energy dissipation: a critical assessment", *Bull. Earthq. Eng.*, **8**(6), 1375-1396.
Mitropoulou, C.C. and Papadrakakis, M. (2011), "Developing fragility curves based on neural network IDA predictions", *Eng. Struct.*, **33**(12), 3409-3421.
Pacific Earthquake Engineering Research (PEER): NGA Database (2005), http://peer.berkeley.edu/smcat/

search.html (last accessed December 2010).
Pagni, C.A. and Lowes, L.N. (2006), "Fragility functions for older reinforced concrete beam-column joints", *Earthq. Spectra*, **22**(1), 215-238.
Pedersen, M.E.H. (2010), "Good parameters for differential evolution", Hvass computer science laboratories Technical Report No. HL1002.
Porter, K., Kennedy, R. and Bachman, R. (2007), "Creating fragility functions for performance-based earthquake engineering", *Earthq. Spectra*, **23**(2), 471-489.
Scott, M.H. and Fenves, G.L. (2006), "Plastic hinge integration methods for force-based beam-column elements", *J. Struct. Eng.*, **132**(2), 244-252.
Scott, B.D., Park, R. and Priestley, M.J.N. (1982), "Stress–strain behaviour of concrete confined by overlapping hoops at low and high strain rates", *ACI J.*, **79**, 13-27.
Shinozuka, M., Feng, M.Q., Lee, J. and Naganuma, T. (2000), "Statistical analysis of fragility curves", *J. Eng. Mech.*, **126**(12), 1224-1231.
Shinozuka, M., Murachi, Y., Dong, X., Zhou, Y. and Orlikowski, M.J. (2003), "Effect of seismic retrofit of bridges on transportation networks", *Earthq. Eng. Eng. Vib.*, **2**(2), 169-179.
Storn, R.M. and Price, K.V. (1997), "Differential evolution - a simple and efficient heuristic for global optimization over continuous spaces", *J. Global Optim.*, **11**, 341-359.
Tantala, M.W. and Deodatis, G. (2002), "Development of seismic fragility curves for tall buildings", *Proceedings of the 15th ASCE Engineering Mechanics Conference*, Columbia University, New York.
Tremblay, R. (2002), "Inelastic seismic response of steel bracing members", *J. Constr. Steel Res.*, **58**(5-8), 665-701.
Vamvatsikos, D. and Cornell, C.A. (2002), "Incremental dynamic analysis", *Earthq. Eng. Struct. Dyn.*, **31**(3), 491-514.
Wen, Y.K. and Ellingwood, B.R. (2005), "The role of fragility assessment in consequence-based engineering", *Earthq. Spectra*, **21**(3), 861-877.

SA